J Therm Anal Calorim (2010) 100:51–56
DOI 10.1007/s10973-009-0187-0

Thermal investigations on phase transformations of Syrian phosphorite: Part I

V. Petkova · V. Yaneva

Received: 11 March 2009 / Accepted: 22 April 2009 / Published online: 19 June 2009

Abstract Syrian phosphorite is subjected to mechanochemical activation carried out in planetary mill. Some phase transformations are ascertained by means of powder XRD and thermal analyses. They reveal as partial transformation of carbonate fluorine apatite into carbonate hydroxyl fluorine apatite and formation of $Ca(PO_3)_2$, as well. The solubility of the activated sample in 2% citric acid is increased as a result of these changes.

Keywords Carbonate-apatite · Thermal analysis · X-ray diffraction

Abbreviations

A	Non-activated Syrian phosphorite
B	Activated for 1,800 s Syrian phosphorite with 20 mm milling bodies of non-alloy steel
C	Activated for 1,800 s Syrian phosphorite with 20 mm milling bodies of Cr–Ni alloy steel
C-F-Ap-$Ca_{10}(PO_4)_6F_{2-2x}(CO_3)_x$	Carbonate fluorine apatite

V. Petkova (✉)
Central Laboratory of Mineralogy and Crystallography,
Bulgarian Academy of Sciences, Sofia,
"Academic G. Bonchev" Str., bl.107,
1113 Sofia, Bulgaria
e-mail: vilmapetkova@gmail.com

V. Yaneva
Technical University—Varna, 1 Studentska Str,
9010 Varna, Bulgaria

Introduction

The rational exploitation of the limited mineral resources together with the provision of strong environmental protection is among the serious challenges for modern society. This necessitates the search of new technologies affording possibilities to process rich as well as poor reserves of mineral resources and to reduce maximally the amount of the wastes. One of the methods allowing utilization of inefficient raw materials is the mechanochemical activation (MA) of natural phosphates. Currently it has turned into a subject of increasing interest as evidenced by the numerous publications devoted to it [1–3].

The results presented here are part of an extensive investigation of the structural and phase transformations in a series of Syrian phosphorite samples, mechanochemically activated in planetary mill Pulverisette–5, Fritsch Co (Germany), activation time from 1.8×10^3 to 1.8×10^4 s, and Cr–Ni alloy steel type milling bodies with a diameter of 0.02 m. These investigations aim at finding out the reasons causing the solubility increase in 2% citric acid of the activated nano-sized samples. The solubility correlates with specific changes in the crystal structure due to the defectiveness of the samples obtained during the mechanochemical activation and the accompanying structural transformations and reactions of solid phase synthesis. The analysis and identification of these processes will provide opportunity to specify the best conditions of MA for preparation of components appropriate for their utilization as slowly acting fertilizers by processing of inefficient raw materials through non-conventional methods.

Analytical procedures

Subject of the study is Syrian phosphorite characterized by the following chemical composition: 29.5 % $P_2O_5^{total}$; 6.9 % $P_2O_5^{ass}$ (in 2% citric acid); 3.2% F; 46.5% CaO; 0.55% R_2O_3 (R = Al, Fe); 1.1% SO_3; 7.3% SiO_2; 0.35% MgO; 0.05% Cl; 6.2% CO_2; moisture content 3.14% and average granulometric particle size of 8×10^{-5} m.

The Syrian phosphorite is represented by phosphate minerals sedimented in seawater conditions. The phosphate ores are complex systems with respect to their mineral composition and in particular to the apatite structure which is inclined for cation and anion isomorphism. According to the structural-chemical classification of Chaikina [3] the Syrian apatite is referred to the group of the "basic" apatite characterized by the ratio $(Ca/P)_{at} = 1.8–1.9$. Such apatite forms in phosphate-calcium systems at pH > 7 and it is characterized by increased defectiveness and isomorphous substitutions within the anionic sub-lattice preliminary by carbonate ions, The main minerals of the Syrian phosphorite are apatite, calcite, and quartz. The apatite is determined as carbonate fluorine type apatite (C–F-Ap) as also ascertained by our previous investigations [2].

The mechanochemical activation was carried out in a planetary mill Pulverisette-5, Fritsch Co (Germany) at a rotating speed of 1.92×10^4 s^{-1}, activation time from 1.8×10^3 to 1.8×10^4 s, type of milling bodies—plain steel, weight of the bodies of 0.510 kg, diameter of the milling bodies of 0.02 m, sample weight 0.020 kg.

In the present work, we used standardized methods for determination of $P_2O_5^{ass}$ following the Bulgarian National Standard 14131-88 and the corresponding EEC Directive 77/535 paragraph 3.1.4 "Extraction of phosphorous soluble in neutral ammonium citrate" as the extraction of $P_2O_5^{ass}$ was performed directly.

Thermogravimetric and differential thermal analyses (TG-DTG-DTA) were performed on a Stanton Redcroft thermal analyzer (England) in the temperature range 293–1350 K, with a heating rate of 0.167 K s^{-1}; the purging gas was 100% clear dry air and flow-rate of $8.33.10^{-7}$ m^3 s^{-1}.

The powder XRD measurements of the samples were performed on a DRON 3 M diffractometer with a horizontal Bragg-Brentano goniometer (radius of 0.192 m) using a Fe-filtered Co-K_α radiation (40 kV, 2.8×10^{-2} A). A step-scan technique was applied with a step size of $0.02^o 2\theta$ and 3 s per step in the range $8–60^o 2\theta$.

Phase identification was performed using the index-file PDF (Powder Diffraction File, ICDD, 2001).

Results and discussion

Chemical analysis

The results of the chemical analysis are presented in Table 1.

The chemical analysis has registered an increment in the solubility in 2% citric acid of sample C of 10% as compared to that one of the non-activated sample (A) and of 6% as compared to analogous sample, however activated with plain steel milling bodies (Table 1). In view of the fact that chemical properties and solubility in particular correlate with the crystal chemical structure of the materials, sample C has been characterized with powder XRD and thermal analyses.

Powder XRD analysis

The results of the powder XRD analysis of sample C are presented in Figs. 1 and 2 and in Table 2.

In contrast to samples A and B the powder XRD pattern of sample C (Table 2, Fig. 1) contains the following new phases: $Ca_{10}(PO_4)_6(OH)F$, $Ca_5(PO_4)_3(OH)$, $Ca_{10}(PO_4)_6CO_3$ and/or $Ca_{10}(PO_4)_5CO_3(OH)F$, and β-$Ca_2P_2O_7$, β-$Ca_3(PO_4)_2$, and β-$Ca(PO_3)_2$. Detection of fluorine apatite, hydroxyl apatite, and/or carbonate hydroxyl fluorine apatite as a mixture in sample C (Fig. 2) evidences partial incorporation of the hydroxyl group in the apatite structure in the positions of the univalent F ion as it has been reported earlier [1, 2] and for relocation of the carbonate group in the vacancies of the Ca ion in the vicinity of the hexagonal axis or in the positions of the F ion on the hexagonal axis, as well [3]. The hydroxyl group incorporation leads to local loss of stability of the apatite structure along the surface of dissolution (211) [4]. The relocation of the carbonate ion is probably related to the formation of carbonate fluorine apatite (C–F-Ap), type A2 [5] or of mixed AB type [1–4, 6–8]. All this introduces additional deformations in the

Table 1 Changes of $P_2O_5^{ass}$, expressed as a percentage from $P_2O_5^{total}$ depending on the construction material of the milling bodies (activation duration 1,800 s)

No.	Samples	Type of milling bodies	Diameter of milling bodies/m	Solubility in 2% citric acid, percentage from $P_2O_5^{total}$/%
1.	*A* Non-activated	–	–	23.5 [2]
2.	*B* Activated for 1,800 s	Plain steel Fe	0.02	28.0 [2]
3.	*C* Activated for 1,800 s	Cr–Ni alloy steel	0.02	34.2

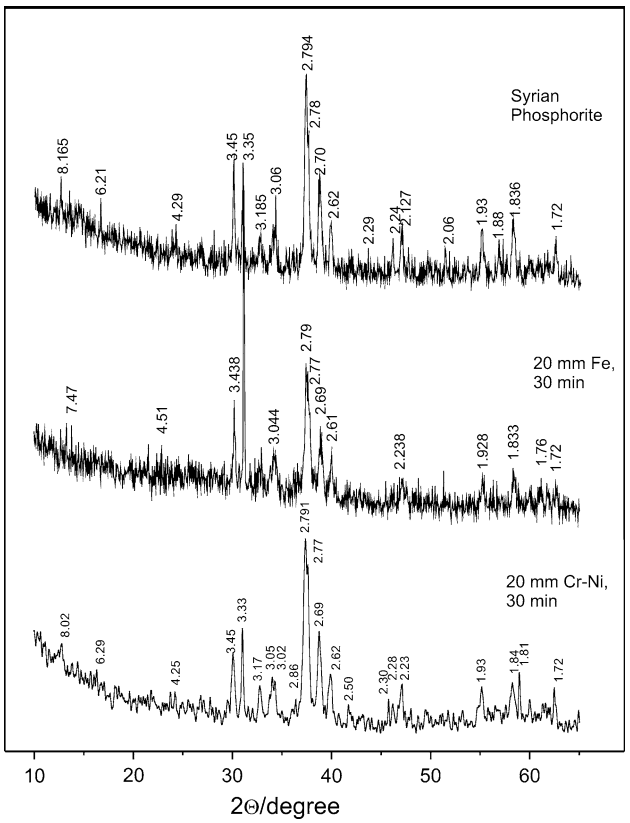

Fig. 1 Powder XRD pattern of Syrian phosphorite samples activated for 1,800 s

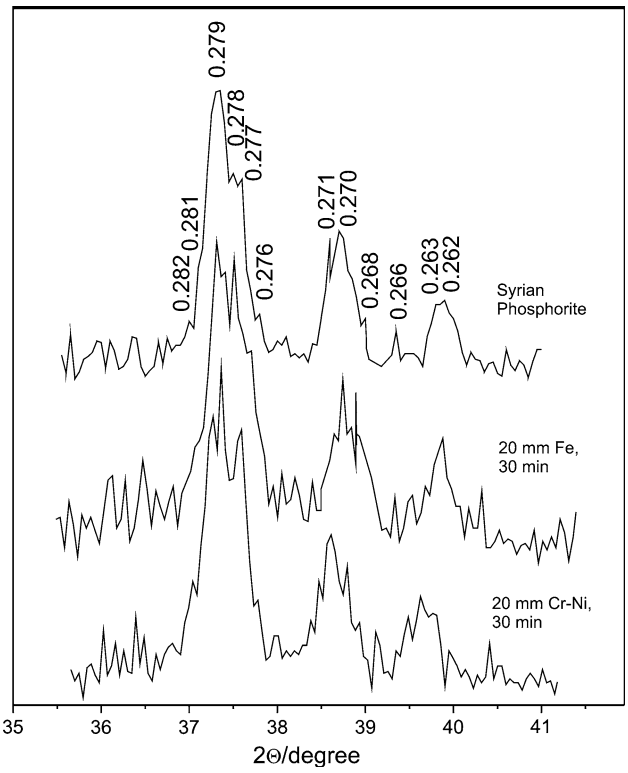

Fig. 2 Powder XRD pattern of Syrian phosphorite samples activated for 1,800 s; the range $d = 0.290–0.262$ nm

apatite structure and its subsequent passing to metastability. More detailed structural analysis will be presented in our coming publication concerning the structural and phase changes of the whole samples' series activated through Cr–Ni milling bodies with diameter of 0.020 m for a period from 1.8×10^3 to 1.8×10^4 s.

The ascertained by means of powder XRD analysis changes in sample C correlate with the results from the chemical analysis. The latter finds out higher solubility of sample C in 2% citric acid as compared to that one for sample A (Table 1).

To demonstrate the validity of the phase transformations in sample C we have used thermal analysis capable to

Table 2 Results from the powder XRD phase analyses

Activation time/s	Identified phases and d/nm
0 [2] (Sample A)	$Ca_5F(PO_4)_3$ (15-0876)–0.344; 0.279*; 0.270; 0.262;
	α-quartz (46-1045)–0.334*, 0.425, 0.182;
	$CaCO_3$ (47-1743)–0.303*, 0.193, 0.187;
1,800 [2] (Sample B)	$Ca_5F(PO_4)_3$ (15-0876)–0.344; 0.279*; 0.2707; 0.262
	α-quartz (46-0145)–0.334*, 0.425, 0.182
	$CaCO_3$ (47-1743)–3.03*, 0.193, 0.187
1,800 (Sample C)	$Ca_5F(PO_4)_3$; α-quartz; $CaCO_3$
	$Ca_5(PO_4)_3(OH)$ (09-0432)–0.281*, 0.277, 0.270
	$Ca_{10}(PO_4)_6(OH)F$ [4]–0.280*, 0.278, 0.271;
	$Ca_{10}(PO_4)_3(CO_3)_3(OH)_2$ (C-OH-Ap) (19-0272)–0.278*, 0.268, 0.346
	$Ca_{10}(PO_4)_5CO_3(OH)F$ (F-C-OH-Ap) (21-0145)–0.271*, 0.281, 0.226
	β-$Ca_2P_2O_7$ (11-0039)–0.302*, 0.322, 0.309
	β-$Ca(PO_3)_2$ (17-0500)–0.374*; 0.352*; 0.301
	β-$Ca_3(PO_4)_2$ (09-0169)–0.288*, 0.261, 0.321

* - Strongest line

register the various isomorphous substitutions within the apatite structure [5–8].

Thermal analysis

The results from the thermal analysis performed on samples A and B presented in details earlier [1] will be used in the present work for more comprehensive interpretation of the registered thermal effects and mass losses on the TG-DTA-DTG curves of sample C (Figs. 3, 4, 5; Table 3).

The analysis of the TG-DTA-DTG dependencies (Figs. 3, 4, 5) in the process of the thermal decomposition of the activated sample C has found increment of the total mass loss of about 0.6% as compared to that one of the non-activated sample A and of 0.9 % as compared with sample B (Table 3). Simultaneously, lowering of the temperature has been registered for the endothermic effect at 1,013 K and new ones have appeared at 685.7, 805.5 K, 1070.6, and 1136.8 K as compared with the curves of the non-activated sample A (Fig. 5).

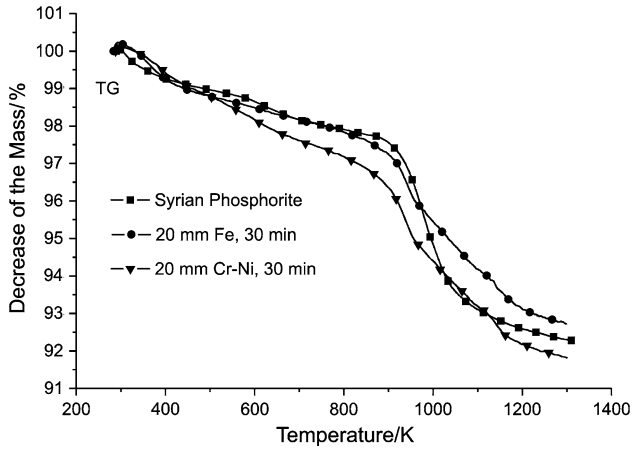

Fig. 3 TG curves of Syrian phosphorite activated for 1,800 s

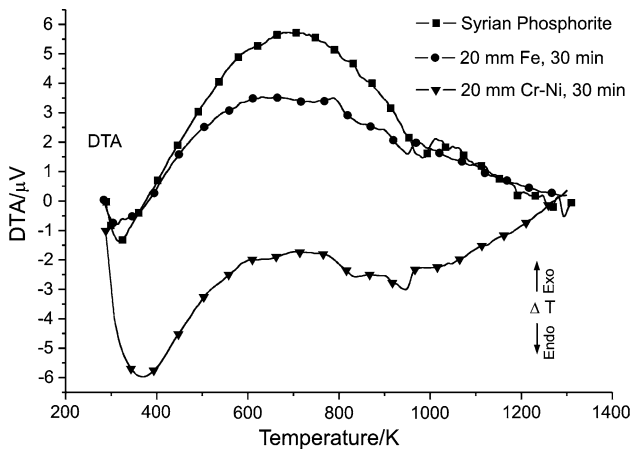

Fig. 4 DTA curves of Syrian phosphorite activated for 1,800 s

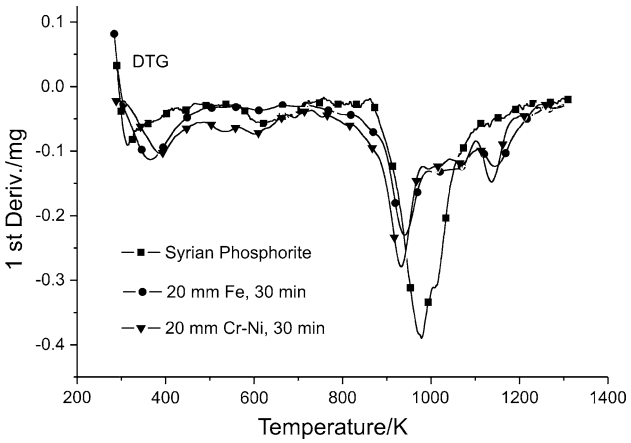

Fig. 5 DTG curves of Syrian phosphorite activated for 1,800 s

The registered endothermic effects and mass losses within the temperature interval 350–485 K have been attributed to the dehydration of the obtained crystalline hydrates obtained as byproducts after the sample activation. Due to the dominant content of C–F-Ap in the activated sample the crystalline hydrates were hard for identification by means of the powder XRD analysis as it was reported earlier [1].

Endothermic effects of low intensity have been registered within the range 570–650 K accompanied by mass losses of 0.3–0.8% (Table 3). As it has also been reported by Ivanova et al. [9] these effects could be explained with the relocation of CO_2^{3-} within the interchannel space in the vicinity of the hexagonal axis at which part of the carbonate ions are liberated in gaseous phase and mass loss is registered.

The endothermic effects within the temperature range 650–700 K (sample C, 685.7 K), could be explained with thermic reaction going between $CaH_2P_2O_7$ and $CaCO_3$ (reaction 1), which was also reported by other authors [7, 8, 10–12]:

$$CaH_2P_2O_7 + 2CaCO_3 = Ca_3(PO_4)_2 + 2CO_2 + H_2O \quad (1)$$

The presence of $CaH_2P_2O_7$ is explained with reaction of solid phase synthesis going during the activation period probably involving aqueous vapor from the reaction media. This means that for sample C the general rule for catenation of P–O–P chains of hydrogenortho- or hydrogen phosphates has been violated (in MA) [13–15]:

$$Ca_{10}F_2(PO_4)_6 + H_2O = CaH_2P_2O_7 + 2Ca_3(PO_4)_2 + 2CaO + CaF_2$$

and/or

$$Ca_{10}F(OH)(PO_4)_6 + H_2O = CaH_2P_2O_7 + 2Ca_3(PO_4)_2 + 3CaO + HF$$

The identification of $CaH_2P_2O_7$ in samples containing SiO_2, is very hard. The strongest diffraction line in the

Table 3 Dynamics of the mass losses upon thermic treatment of Syrian phosphorite up to 1350 K depending on the construction material of the milling bodies

No	Activation time/s						
	Initial phosphorite (sample A) [1]		1,800 (sample B) [1]		1,800 (sample C)		Reaction
	T/K	ΔG/ %	T/K	ΔG/ %	T/K	ΔG/ %	
1.	313.2 (291.9–350.3)	0.6	314.3 (296.6–324.7)	0.2	–	–	Dehydrataion
2.	372.8 (350.3–418.0)	0.3	367.4 (324.7–486.8)	1.2	389.9 (302.2–485.8)	1.3	Dehydrataion
4.	438.5 (418.0–476.1)	0.2	–	–	–	–	Organic component combustion
5.	605.2 (557.6–733.4)	0.8	619.2 (566.6–669.1)	0.3	607.4 (566.8–669.8)	0.7	Partial decarbonization
	–	–	–	–	685.7 (669.8–715.6)	0.3	Reaction 1, $CaH_2P_2O_7$ to $Ca_3(PO_4)_3$
6.	–	–	801.0 (759.4–834.5)	0.2	805.5 (780.3–831.8)	0.3	Dehydrataion of $Ca(OH)_2$
7.	–	–	866.1 (834.5–891.8)	0.4	–	–	Decarbonization of A type carbonate apatite
8.	977.1 (860.4–1002.3)	2.8	938.0 (891.8–978.9)	1.6	935.1 (831.8–993.8)	2.5	Decarbonization of B type carbonate apatite
9.	1013.9 (1002.3–1101.3)	1.7	1002.3 (978.9–1038.8)	0.8	1002.2 (993.8–1034.4)	0.5	Decarbonization of calcite
10.	–	–	1063.3 (1038.8–1104.2)	0.8	1070.6 (1034.4–1104.8)	0.8	Reaction 3, $Ca_4P_2O_9$
11.	–	–	1143.8 (1104.2–1204.2)	1.0	1136.8 (1104.8–1196.8)	1.0	Reaction 4, 5, 6 $Ca_3(PO_4)_2$, Ca_2SiO_4
Total		7.8		7.5		8.4	

powder XRD pattern of $CaH_2P_2O_7$ is $d = 0.334$ nm (PDF 51-0200). It coincides with the strongest SiO_2 line (PDF 46-1045), which dominates in the powder XRD patterns of the activated nano-sized samples (Fig. 1) [2]. The other strong lines having $d = 0.376$ nm and $d = 0.318$ nm are very weak to be detected. This is why hydro-pyrophosphate has not been identified by the powder XRD analysis (Fig. 1). This however becomes possible by thermal decomposition of the activated samples and registration of the corresponding indicative thermic effects in the range 650–700 K, which are missing for the non-activated Syrian phosphorite [1].

Within the temperature range 717–854 K a new endothermic effect at 805.5 K has been detected for the activated sample C which is accompanied by mass loss of about 1%. The latter is assigned to the thermal decomposition of $Ca(OH)_2$, obtained as a byproduct after the activated sample has absorbed atmospheric water.

Two endothermic effects have been detected within the temperature range 850–1,000 K on the DTA curve of sample C analogous to those registered within the temperature range 970–1,015 K for samples A and B [1]. These effects have been referred to liberation of the carbonate ions from the carbonate fluorine apatite type B and from calcite (Table 3). It is suggested that as a result of the activation, the decomposition of the structurally bound in the apatite framework carbonate ions has been accelerated and it has occurred at lower temperature range as compared to that one for the non-activated sample A [1]. No effect related to the decomposition of the carbonate ions from C–F-Ap type A2 [5] or from mixed type AB [3], has been registered for sample C as it has been evidenced for sample B [2].

Most likely, within the same temperature range $Ca(PO_3)_2$, obtained upon the mechanochemical activation has transformed into pyrophosphate following the reaction (2):

$$Ca(PO_3)_2 + CaO = Ca_2P_2O_7$$

and/or

$$Ca(PO_3)_2 + CaCO_3 = Ca_2P_2O_7 + CO_2 \quad (2)$$

The registered new endothermic effect within the temperature range 1,000–1,100 K, which misses at the decomposition of non-activated Syrian phosphorite (sample A), is referred to the decomposition of $Ca_{10}(PO_4)_6(OH)F$ following the reaction (3):

$$Ca_{10}(PO_4)_6(OH)F = 2Ca_3(PO_4)_2 + Ca_4P_2O_9 + HF \quad (3)$$

The formation of $Ca_4P_2O_9$ under the conditions of thermal analysis was evidenced earlier [1].

Several reactions have probably been responsible for the mass losses and the new endothermic effect registered within the last temperature range 1,100–1,200 K:

$$Ca_{10}(PO_4)_6(OH)_2 + 0.5SiO_2 = 3Ca_3(PO_4)_2 + 0.5Ca_2SiO_4 + H_2O \quad (4)$$

$$CaO + SiO_2 = CaSiO_3 \quad (5)$$

$$Ca_2P_2O_7 + CaO = Ca_3(PO_4)_2 \quad (6)$$

The product from the thermal heating of activated nanosized sample from natural apatite contains mainly $Ca_3(PO_4)_2$, and certain amounts of $Ca_4P_2O_9$ and calcium silicates—Ca_2SiO_4 and $CaSiO_3$, as well. The decomposition has been accompanied by structural stabilization and relaxation of the accumulated mechanical energy.

Similar changes with the attendant on the apatite mineral α-quartz have not been detected. Taking into consideration the high hardness of this mineral, no reactions have been expected for it during the activation period.

Comparing the results from the MA of samples from Syrian phosphorite treated for 1.8×10^3 s with 0.02 m Fe [1] and Cr–Ni milling bodies, a similarity in the registered stages of thermal decomposition has been found. Weak decrease of the temperature ranges has been detected for the thermic effects of samples activated with chrome-nickel alloy steel. The result seems logically sound since the Cr-Ni milling bodies have bigger density which leads to better expressed efficiency of the performed activation.

Conclusions

The obtained results from the chemical, powder XRD and thermal analyses for the sample activated for 1,800 s through Cr–Ni steel milling bodies give ground to make the following conclusions:

Substantial structural and phase changes have been registered upon the chosen conditions for mechanochemical activation as most strongly they have been expressed for the carbonate fluorine apatite and the calcite. They are referred to the partial transformation of carbonate fluorine apatite into carbonate hydroxyl fluorine apatite. The use of heavier and denser milling bodies leads to strongly expressed structural changes within the apatite structure and phase transformations yielding $CaH_2P_2O_7$ and $Ca(PO_3)_2$ as run products of the MA. During the present study no evidence has been obtained for isomorphous substitution incorporating carbonate ions in vacancies of the calcium ions on or in the vicinity of the hexagonal axis (carbonate fluorine apatite of type A2 and carbonate fluorine apatite of the mixed type AB).

Based on the results from the powder XRD and thermal analyses it can be assumed that the increased solubility of the activated sample C in 2% citric acid found out by the chemical analysis is a logical sequence of the phase changes occurring during the activation period.

Acknowledgement The authors thank the National Fund "Scientific research" of the Ministry of Education for the financial support (project DOO2-104).

References

1. Petkova V, Yaneva V. Thermal behavior and phase transformations of nanosized apatite (Syria). J Therm Anal Calorim (in press).
2. Yaneva V, Petrov O, Petkova V. Structural and spectroscopic studies of the nanosize appatite (Syrian). Mater Res Bull. 2009;44:693–9.
3. Chaikina MV. In: Avvakumov EG, editor. Mechanochemistry of natural and synthetic apatites. Novosibirsk: Publishing house of SB RAS, Branch "GEO"; 2002. pp. 11–5; 105–7; 114–5; 139 (in Russian).
4. Tõnsuaadu K, Rimm K, Veiderma M. Composition and properties of thermophosphates from apatite and aluminosilicates. Phosphorus Sulfur Silicon Related Elements. 1993;84(1–4): 73–81.
5. Chrisis Tacker R. Carbonate in igneous and metamorphic fluorapatite: two type A and two type B substitutions. Amer Mineralogist. 2008;93:168–76.
6. Bianco Al, Cacciotti Il, Lombardi M, Montanaro L, Gusmano G. Thermal stability and sintering behaviour of hydroxyapatite nanopowders. J Therm Anal Calorim. 2007;88:237–43.
7. Tõnsuaadu K, Peld M, Bender V. Thermal analysis of apatite structure. J Therm Anal Calorim. 2003;72(1):363–71.
8. Lafon JP, Champion E, Bernache-Assollant D, Gibert R, Danna AM. Thermal decomposition of carbonated calcium phosphate apatites. J Therm Anal Calorim. 2003;73:1127–34.
9. Ivanova TI, Frank-Kamenetskaya OV, Kol'tsov AB, Ugolkov VL. Crystal structure of calcium-deficient carbonated hydroxyapatite. J Solid State Chem. 2001;160:340–9.
10. Tõnsuaadu K, Peld M, Leskela T, Mannonen R, Niinisto L, Veiderma M. A thermoanalytical study of synthetic carbonate-containing apatites. Thermochim Acta. 1995;256:55–65.
11. Trojan M, Brandová D. Synthesis of binary cyclo-tetraphosphates by thermal decomposition of polyphosphate glasses. J Therm Anal Calorim. 1990;36:2075–8.
12. Trojan M, Šulcová P, Sýkorová L. Thermal analysis of Ba(II)–Sr(II) cyclo-tetraphosphates(V). J Therm Anal Calorim. 2002;68:75–9.
13. Dohnalová Ž, Šulcová P, Trojan M. Synthesis and characterization of $LnFeO_3$ pigments. J Therm Anal Calorim. 2008;91:559–63.
14. Petkova V, Pelovski Y, Dombalov I, Tonsuaadu K. Thermochemical investigations of natural phosphate with ammonium sulphate additive. J Therm Anal Calorim. 2005;80:701–8.
15. Petkova V, Pelovski Y, Dombalov I, Kostadinova P. Influence of triboactivation conditions on the synthesis in natural phosphate-ammonium sulphate system. J Therm Anal Calorim. 2005;80: 709–14.